NASA TECHNICAL REPORT

NASA TR R-219

NASA TR R-219

CHARACTERISTICS OF A CONTINUOUS-FLOW INDUCTION PLASMA ACCELERATOR

by J. D. Brooks, W. D. Beasley, and R. L. Barger

Langley Research Center
Langley Station, Hampton, Va.

NATIONAL AERONAUTICS AND SPACE ADMINISTRATION • WASHINGTON, D. C. • FEBRUARY 1965

CHARACTERISTICS OF A CONTINUOUS-FLOW INDUCTION PLASMA ACCELERATOR

By J. D. Brooks, W. D. Beasley, and R. L. Barger

Langley Research Center
Langley Station, Hampton, Va.

NATIONAL AERONAUTICS AND SPACE ADMINISTRATION

For sale by the Office of Technical Services, Department of Commerce, Washington, D.C. 20230 -- Price $2.00

CHARACTERISTICS OF A CONTINUOUS-FLOW INDUCTION PLASMA ACCELERATOR

By J. D. Brooks, W. D. Beasley,
and R. L. Barger
Langley Research Center

SUMMARY

Characteristics of continuous-flow induction plasma accelerators with a 10-kilocycle, single-phase driving coil on supersonic nozzles were studied. Pressure measurements and vane-deflection measurements were made in a 15-centimeter-diameter accelerator at various mass flow rates. Charged-particle velocities were obtained in 15-centimeter-diameter and 10-centimeter-diameter accelerators by measuring with photoelectric detectors the time required for a change in flow luminosity to travel a known distance.

Pressure-probe measurements indicated that the entire flow, including the boundary layer and the separated-flow region, was accelerated in the 15-centimeter-diameter accelerator. The largest increase in pitot pressure was 250 percent of the cold-flow value with 20 kilowatts of 10-kilocycle driving power. The charged-particle velocities increased as the mass flow rate was reduced and as the power was increased. The maximum charged-particle velocity obtained was 40,000 meters per second in the 10-centimeter-diameter accelerator. Average velocity and thrust obtained from vane-deflection measurements were in good agreement with those obtained from pressure-probe measurements.

INTRODUCTION

The electromagnetic acceleration of a plasma to extremely high velocities has been accomplished both with and without electrodes in contact with the plasma. Several methods have been investigated which produce a high-velocity transient flow, such as the electromagnetic shock tubes described in reference 1 and the coaxial electrodes described in reference 2. High-velocity continuous flows without electrodes are produced by the induction plasma accelerators of references 3 to 5. Such flows have been produced with use of electrodes by the crossed-field accelerators described in references 6 and 7. Electromagnetic accelerators using electrodes in contact with the plasma have the disadvantage of introducing impurities into the gas from the electrodes.

The experimental investigation of this paper is part of the basic research effort in the area of plasma acceleration of the National Aeronautics and Space

Administration, with particular emphasis on a continuous-flow, electrodeless, induction plasma accelerator. The configurations investigated combine an accelerator driving mechanism, similar to the device described in reference 3, with supersonic nozzle expansions so that a high-velocity cold flow is present prior to starting the accelerator. Previous experimental investigations have utilized an ionization source for maintaining the plasma. However, with the design of this investigation, the ionization source was used only to start the discharge. Pressure and velocity measurements are analyzed to provide a detailed description of the flow and the overall properties of the accelerator, thereby providing a basis for assessing the potential capabilities of such an accelerator when not subject to the power limitations of the present laboratory-scale device.

The primary accelerator component was a 10-kc, single-phase driving coil with a laminated iron core. Pressure measurements, vane deflections, and charged-particle velocities were obtained in a 15-cm-diameter accelerator at mass flow rates from 0.035 g/sec to 0.940 g/sec. Charged-particle velocities were obtained in the 10-cm-diameter accelerators at mass flow rates from 0.008 g/sec to 0.080 g/sec. Argon gas was used in these accelerators.

SYMBOLS

A cross-sectional area between core and outer wall at vane location, square centimeters

A_v area of face of vane, 1 square centimeter

A^* cross-sectional area of nozzle throat, square centimeters

F thrust, dynes

F_m momentum thrust, dynes

F' thrust per unit area, dynes per square centimeter

F_i thrust based on charged-particle velocity, dynes

g gravitational acceleration constant, 980 centimeters per second per second

K correction factor for radial variation in velocity at vane location, 0.67 for present investigation

k correction factor converting millimeters Hg to grams per square centimeter, 1.36

M Mach number

$\dot{m}$ mass flow rate, grams per second

p	static pressure measured at wall, millimeters of Hg
p_a	outside or ambient pressure, 0 in outer space
p_t	total pressure, measured in stagnation chamber, millimeters of Hg
p_t'	pitot pressure, measured total pressure in flow, millimeters of Hg
r	radius, from center line of accelerator, centimeters
V	velocity, meters per second
w	weight of vane, 1.9 grams
γ	ratio of specific heats, 1.67 for argon gas
ρ	gas density, grams per cubic centimeter
θ	angle of deflection of vane from vertical, degrees

Subscript:

max	maximum

APPARATUS AND PROCEDURE

Plasma Accelerators

A 15-cm-diameter plasma accelerator was used so that pitot-pressure surveys could be made across the stream with a large-diameter pitot-pressure tube without choking the flow. Three 10-cm-diameter plasma accelerators were utilized so that the induced voltage could be increased. The only difference in the 10-cm-diameter accelerators was the diameter of the throat which changed the Mach number by changing the cross-sectional area of the nozzle throat. The cross-sectional areas of the nozzle throats were 0.57 sq cm for the 15-cm-diameter accelerator and 0.31 sq cm, 0.51 sq cm, and 4.25 sq cm for the 10-cm-diameter accelerators. Schematic drawings of the 15-cm- and 10-cm-diameter plasma accelerators (also referred to as 15-cm accelerator and 10-cm accelerator) are shown in figures 1 and 2, respectively, and photographs of these accelerators are shown as figure 3. The 10-cm-diameter accelerator is shown connected to the vacuum system.

The circular expansion cones of the plasma-accelerator nozzles are made from pyrex tubing and have expansion angles of 20°. A laminated iron core was mounted coaxially through each accelerator; in the 10-cm-diameter accelerators the laminated iron core was supported in the settling chamber and in the vacuum chamber to avoid choking the flow. The core consisted of a bundle of 0.6-mm-diameter wires in a 5-cm-diameter quartz tube. The iron core was located with one end at the nozzle throat and extended for a distance of 30.48 cm downstream.

A silicone rubber plug in the quartz tube at the upstream end of the core prevented the core from moving in an upstream direction when the accelerator was energized. The upstream end of the quartz tube was vented to the settling chamber. Argon gas was introduced uniformly into the settling chamber.

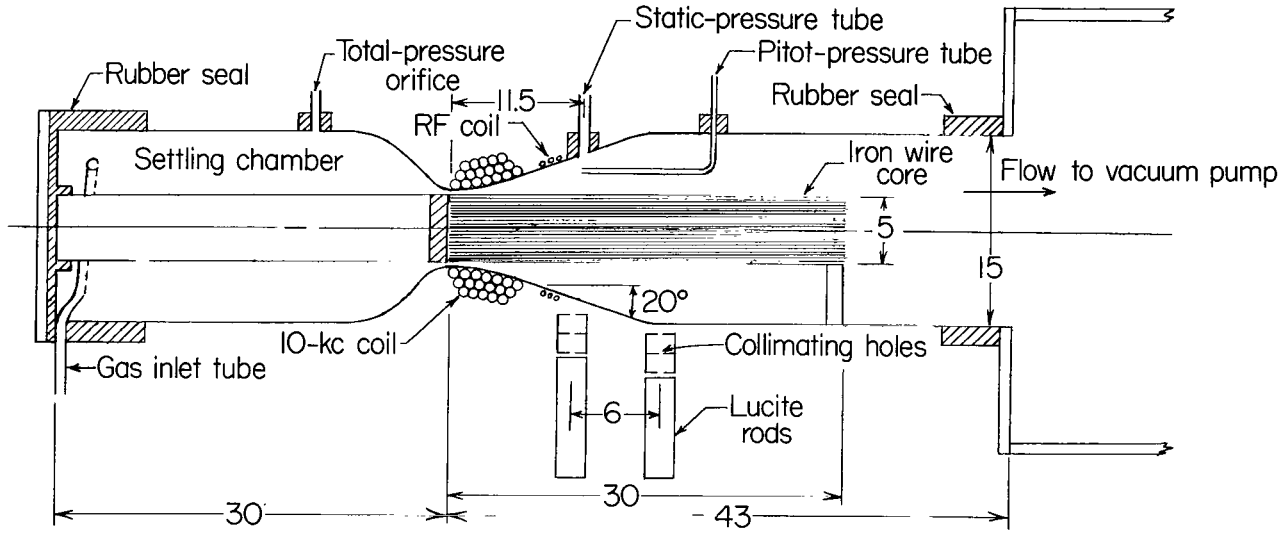

Figure 1. - Schematic diagram of the 15-cm-diameter induction plasma accelerator. All dimensions are in centimeters unless otherwise noted. (Not to scale.)

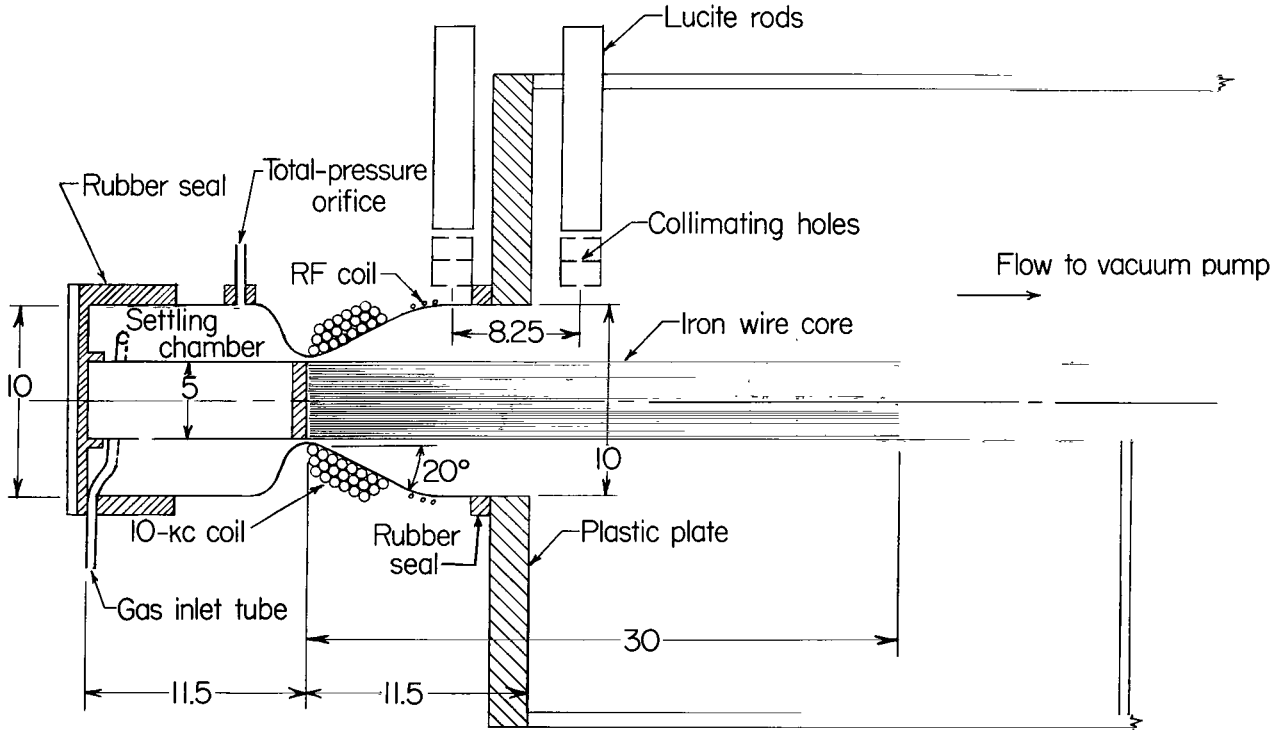

Figure 2. - Schematic diagram of the 10-cm-diameter induction plasma accelerator. All dimensions are in centimeters unless otherwise noted. (Not to scale.)

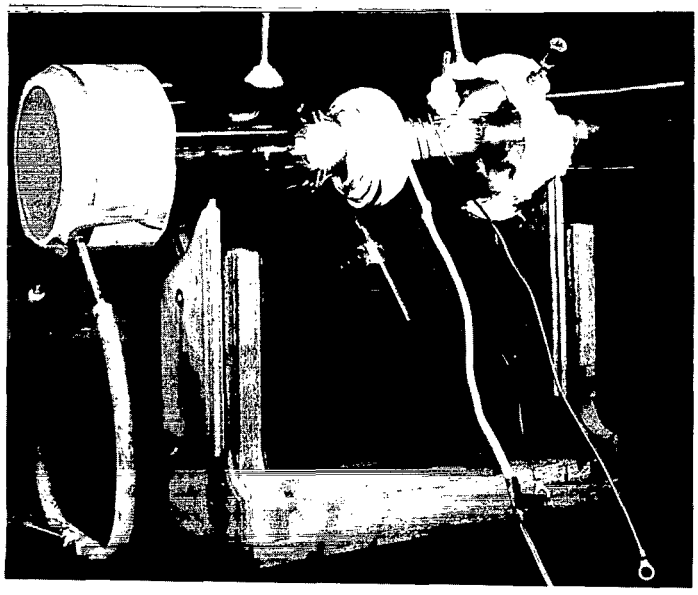

(a) The 15-cm-diameter accelerator. L-63-7741

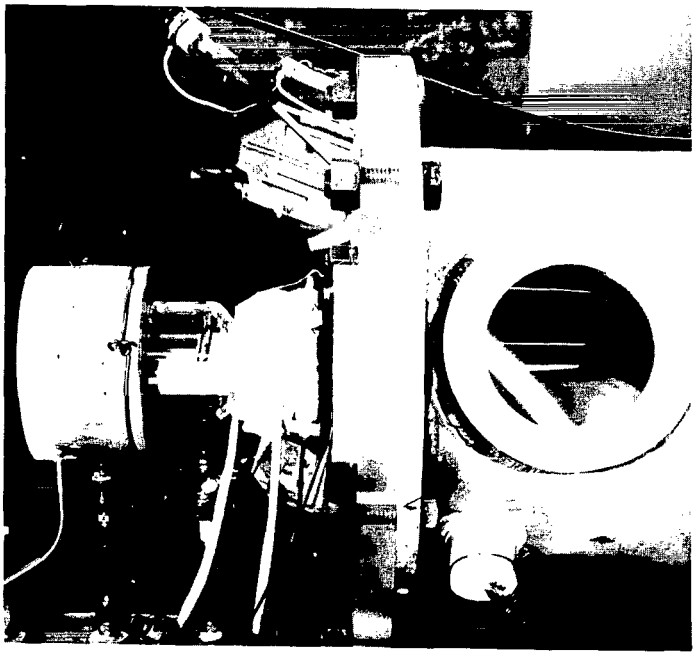

L-63-3362

(b) The 10-cm-diameter accelerator connected to the vacuum system.

Figure 3. - Photographs of plasma accelerators studied.

The 10-kc drive coils were wound on the conical sections of the nozzles as shown in figures 1 and 2. The coils were water cooled and had 18 turns of 0.64-cm-diameter insulated copper tubing for the 15-cm accelerator and 20 turns for the 10-cm accelerators. A 30-Mc radio-frequency starting coil was mounted just downstream from the 10-kc drive coil. The power required from the 30-Mc oscillator for starting the discharge was generally less than 500 watts.

The 10-kc, single-phase power required to drive the accelerator was obtained from a 30-kW-motor generator in which the output voltage was variable from 0 to 880 volts rms. The power output was dependent on the load and the set voltage. The drive coil was connected in a parallel resonant circuit which required a capacitor of approximately 5.7 μF and an inductance of approximately 44 μH.

Vacuum System

The vacuum system consisted of a vacuum chamber connected to a heat exchanger and then to a mechanical booster pump. The 10-cm plasma accelerator is shown connected to the vacuum chamber in figures 2 and 3. The mechanical booster pump had a pumping capacity of 75,000 to 100,000 liters/min over the operating range, which was adequate to maintain supersonic flow.

Instrumentation and Measurements

Total pressure was measured in the settling chamber with an aneroid gage that is accurate within 2 percent. Static pressure was measured at the wall of the accelerators, 11.5 cm downstream from the throat, through an orifice with an inside diameter of 0.47 cm. In the 15-cm accelerator, at the same location, pitot-pressure measurements were made across the stream (between the core and the outside wall) by using a 0.47-cm-diameter, stainless-steel, open-end, total-pressure tube with an inside diameter of 0.32 cm. Static pressure and pitot pressure were measured with thermocouple vacuum gages that were calibrated in both air and argon gas. The accuracy of the pressure measurements is estimated to be within 5 percent for air and within 8 percent for argon gas. The thermocouple pressure sensors were located within 7.6 cm of the wall of the accelerator to reduce the lag time, and the pitot-pressure sensor was attached to a block of metal which served as a heat sink to prevent overheating. The metal shields of the thermocouple pressure sensors were grounded, and shielded wiring and a filter circuit were used to prevent interference from the 10-kc drive coil or the 30-Mc radio-frequency coil.

At high mass flow rates, the pitot-pressure measurements made in the 15-cm accelerator near the center of the stream in a continuum flow are accurate within the accuracy of the instrumentation. The pitot-pressure measurements made in the boundary layer at high mass flow rates, all measurements made at low mass flow rates, and static-pressure measurements made at the wall are in some error because the flow is in either the slip-flow region or the transition region to free-molecule flow. From the results of reference 8 the total error is believed to be less than 10 percent at high mass flow rates (above 0.25 g/sec) but somewhat greater at low mass flow rates.

The method used to measure the charged-particle velocity was similar to the technique described in reference 9. The 10-kc drive coil induces an increase in luminosity in the stream 20,000 times per second (once each half-cycle). The change in light intensity was observed through 0.8-mm-diameter collimating holes by photomultipliers at various downstream locations as shown in figures 1 and 2. The photomultipliers were connected to a dual-beam oscilloscope. Since the photomultiplier near the coils observed the change in light intensity before the other photomultiplier, the respective oscilloscope traces were displaced. This displacement represents a time lapse that can be used with the known collimator spacing to compute the longitudinal velocity of the charged particles.

The vane (or pendulum) was made of a dielectric material (glass-bonded mica) and was located in the center of the stream 11.5 cm downstream from the throat. The area of the face of the vane was 1 sq cm and the total weight of the vane was 1.9 g.

Vane-deflection measurements were obtained in the 15-cm plasma accelerator by photographing the vane in the deflected position before and after the accelerator was turned on. Since the disturbance produced by the initiation of the discharge caused a transient oscillation of the vane, the accelerator was run for several seconds to permit the oscillation to die out before photographs were taken.

The mass flow rate of the argon gas was determined by running the gas through a calibrated sonic orifice and measuring the pressure upstream with an aneroid gage. The mass-flow-rate measurements are estimated to be accurate within 5 percent at the high mass flow rates used in the 15-cm-diameter accelerator. The error is believed to be somewhat larger at the low mass flow rates used in the 10-cm-diameter accelerators.

Procedure

Pressure measurements, charged-particle velocities, and vane deflections were obtained in the 15-cm accelerator within the range of mass flow rates from 0.035 g/sec to 0.940 g/sec. In the 10-cm accelerator only charged-particle velocities were obtained over the range of mass flow rates from 0.008 g/sec to 0.080 g/sec.

The procedure followed in obtaining these data was to set the desired mass flow rate of argon gas through the accelerator. The radio-frequency oscillator was started, causing a bright discharge in the accelerator tube; then the 10-kc drive coil was energized and set at the desired power level. Since the radio-frequency oscillator (ionization source) was not needed to sustain the accelerator discharge, it was turned off before measurements were made. The addition of the 10-kc driving power increased the intensity of the discharge and caused the discharge to extend downstream. Turning off the radio-frequency ionization source had no apparent effect on the intensity of the discharge or on the measurements, perhaps because the radio-frequency power was low compared with the 10-kc driving power. A test generally did not exceed 10 to 20 sec, since the accelerator core was not water cooled and the change in the permeability of the iron as it became hot would detune the 10-kc circuit at high power levels.

RESULTS

The pitot-pressure profiles measured across the stream in the 15-cm accelerator are presented in figure 4. The variation of 10-kc driving power, maximum pitot pressure, and static wall pressure with mass flow rate in the 15-cm accelerator is shown in figure 5 at three values of the drive voltage. In figure 6, the variation of the pressure ratio $(p_t')_{max}/p$ with mass flow rate in the 15-cm accelerator is presented. The charged-particle velocities measured in the 15-cm accelerator by means of two photomultipliers placed longitudinally along the direction of flow are given in figure 7. The variation of mean free path of the neutral particles with mass flow rate, from reference 10, is shown in figure 8. The charged-particle velocities measured in the 10-cm accelerators are presented in figure 9 and typical oscilloscope traces obtained with the photomultipliers are given in figure 10.

For comparison, the ideal thrust F_i that could be obtained from the plasma accelerators on the assumption that the entire flow is moving at the charged-particle velocity was determined by using the following equation for the total thrust as given in reference 11:

$$F = 100\dot{m}V + Akg(p - p_a)$$

The first term of the right-hand side of the equation is the momentum thrust and the second term is the pressure thrust. The outside or ambient pressure p_a was assumed to be zero as in outer space. The results are presented for the 15-cm and for the 10-cm accelerators in figures 11 and 12, respectively.

The actual thrust of the 15-cm accelerator was determined from the vane-deflection measurements and from the pitot-pressure measurements. In both methods a uniform distribution of velocities about the circumference was assumed.

The formula used with the vane-deflection measurements is similar to that used in reference 12. The momentum thrust per unit area at the vane is

$$F' = g \frac{w}{A_v} \frac{\tan \theta}{\cos \theta}$$

The total thrust of the accelerator can be approximated by

$$F = Ag\left[K \frac{w}{A_v} \frac{\tan \theta}{\cos \theta} + k(p - p_a)\right]$$

where A is the total cross-sectional area of the flow and K is a factor that accounts for the radial nonuniformity of the flow. The factor K was estimated to be 0.67; this value was found by integrating the hot-flow pitot-pressure profiles in figure 4 and obtaining an average pressure for each profile. For each profile a ratio of the average value to the maximum value was determined and then the factor K was found by averaging these ratios. This averaging process assumes that the momentum thrust $F_m = kg\gamma ApM^2$ (ref. 11) is proportional to the pitot pressure. That this assumption is approximately true for Mach numbers above 1 is indicated by the fact that a plot of p_t' against M^2 is virtually linear for this range of Mach numbers. The difference in the radial-flow distribution from hot flow to cold flow was not considered in detail and the value of K was assumed to be the same for both cold and hot flows. Thrust values obtained from vane-deflection measurements are presented in figure 11.

Thrust was also found from the radial pitot-pressure measurements by determining the rate of change in momentum from the settling chamber to the pitot-pressure-tube location and adding the pressure thrust. The equation used was

$$F = kg\left[\gamma \int pM^2 dA + \left(p - p_a\right)A\right]$$

Equilibrium flow with a specific-heat ratio γ of 1.67 was assumed. These thrust results are also shown in figure 11.

The momentum thrust is not constant over the cross section but can be expressed by the integral

$$F_m = 10^4 \int \rho V^2 dA$$

This momentum thrust has been approximated by the methods previously described and is plotted in figure 11(a).

Furthermore, the mass rate of flow is not uniform over the cross section in the region in which the measurements were made. It, too, can be written as an integral

$$\dot{m} = \int \rho V \, dA$$

A velocity averaged with respect to mass rate of flow can be defined by

$$V = \frac{\int \rho V^2 dA}{\int \rho V \, dA}$$

where the numerator is obtained by multiplying the momentum-thrust values in figure 11(a) by the gravitational acceleration constant g and the denominator is simply the measured total mass flow rate. The average velocities, obtained by this procedure, in the 15-cm accelerator are presented in figure 7.

DISCUSSION

Accelerator Design

The design of the induction plasma accelerator with the annular supersonic nozzle and the 10-kc driving coil located on the diverging section (figs. 1 and 2) is superior to the preliminary configuration used in reference 3. The design used in reference 3 had a step increase in diameter at the 10-kc-coil location and no flow prior to starting the accelerator. The accelerator was difficult to operate without mercury vapor and would not operate when the radio-frequency preionizing coil was turned off. The present accelerator had to be started by the radio-frequency coil and continued to perform stably after the radio-frequency coil was turned off.

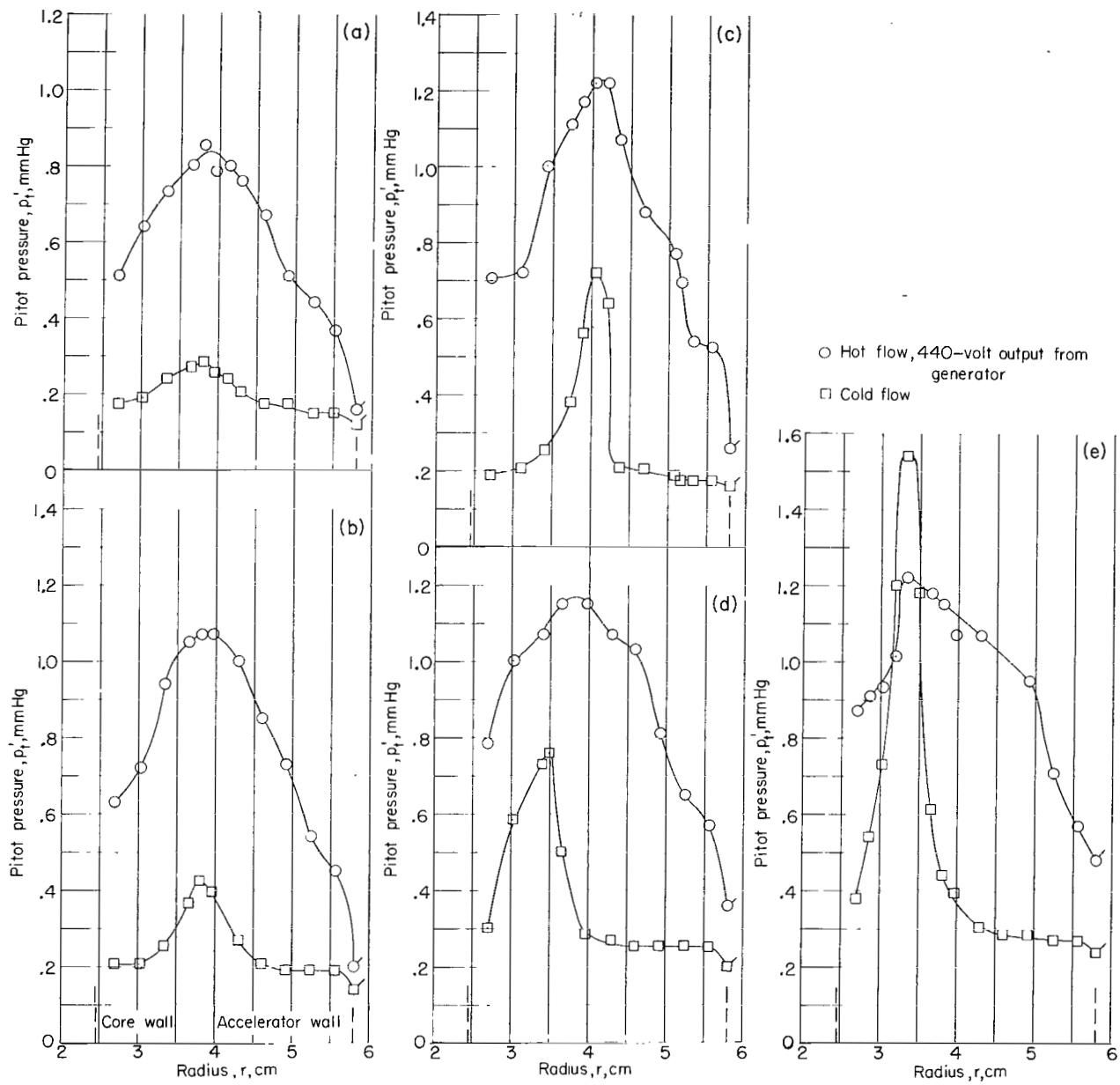

(a) $\dot{m}$ = 0.310 g/sec; p_t = 20 mm Hg.

(b) $\dot{m}$ = 0.413 g/sec; p_t = 25 mm Hg.

(c) $\dot{m}$ = 0.518 g/sec; p_t = 30 mm Hg.

(d) $\dot{m}$ = 0.623 g/sec; p_t = 35 mm Hg.

(e) $\dot{m}$ = 0.727 g/sec; p_t = 40 mm Hg.

Figure 4. - Pitot-pressure profiles at various mass flow rates, across the stream in the 15-cm-diameter plasma accelerator. (Symbols with ticks indicate static pressure at wall.)

The principle of operation of the induction plasma accelerator is similar to that utilized in the well-known laboratory experiment demonstrating the electromagnetic repulsion of a metal ring (ref. 13). In the present accelerator, a 10-kc coil induces current in the preionized gaseous secondary instead of in a metal ring. The induced current in the gaseous secondary is out of phase with that in the 10-kc primary coil so that the charged particles are driven away from the coil.

Since the neutral-gas acceleration is due to collisions between the high-velocity charged particles and the neutral-gas particles, the present design is believed to be superior to the preliminary design of reference 3 because the neutral-gas velocity is generally supersonic before the accelerator is started. The coupling between the 10-kc drive coil and the plasma is also better, particularly at the small end of the diverging nozzle where the gap between the primary coil and the iron core is approximately 4 mm.

Pressure Measurements

Because of the uncertainty of making pressure measurements in low-density plasma flows, the pitot-pressure profiles were obtained in the 15-cm accelerator with a 4.7-mm-diameter probe. According to information given in reference 14 (for air) and in reference 15 (for nitrogen at 3000° K), the error in pitot-pressure measurements due to viscous effects at low probe Reynolds number increases with decreasing pressure. In the 15-cm accelerator the error due to viscous effects is negligible at mass flow rates above 0.25 g/sec but increases rapidly at the lower mass flow rates corresponding to the lower pressures. Hence, the pressure data are considered only qualitatively correct at the lower mass flow rates and are not analyzed in detail. Furthermore, the pressures measured in the hot flow are average values resulting from the high-velocity charged particles and the low-velocity neutral gas.

Except for the peak value at the highest mass flow rate (0.727 g/sec), the pitot-pressure profiles in the 15-cm accelerator (fig. 4) show an increase in pitot pressure when the 10-kc drive coil is energized. The cold-flow profiles indicate that a relatively thick boundary layer builds up on the inner wall and that the flow separates from the outer wall as it expands through the nozzle. In the hot-flow profiles, the boundary layer near the core and the separated flow on the outer wall have clearly been accelerated. In both the cold and hot flows the peak pressures occur generally near the core or inner wall. The flow distribution in cold flow could be improved considerably by dispensing with the core. However, the core increases the efficiency of the accelerator by increasing the voltage induced in the gas and also by improving the shape of the magnetic-field distribution. Tests have indicated that the accelerator will operate without the core, but only over a narrow pressure range and only when the radio-frequency coil is left on to maintain the ionization.

The data shown in figure 5 were obtained in the 15-cm accelerator with constant voltage settings on the 10-kc drive coil. Increasing the voltage from 330 volts to 400 volts resulted in an increase in power output from the generator of about 50 percent, and increasing the voltage from 330 volts to 440 volts

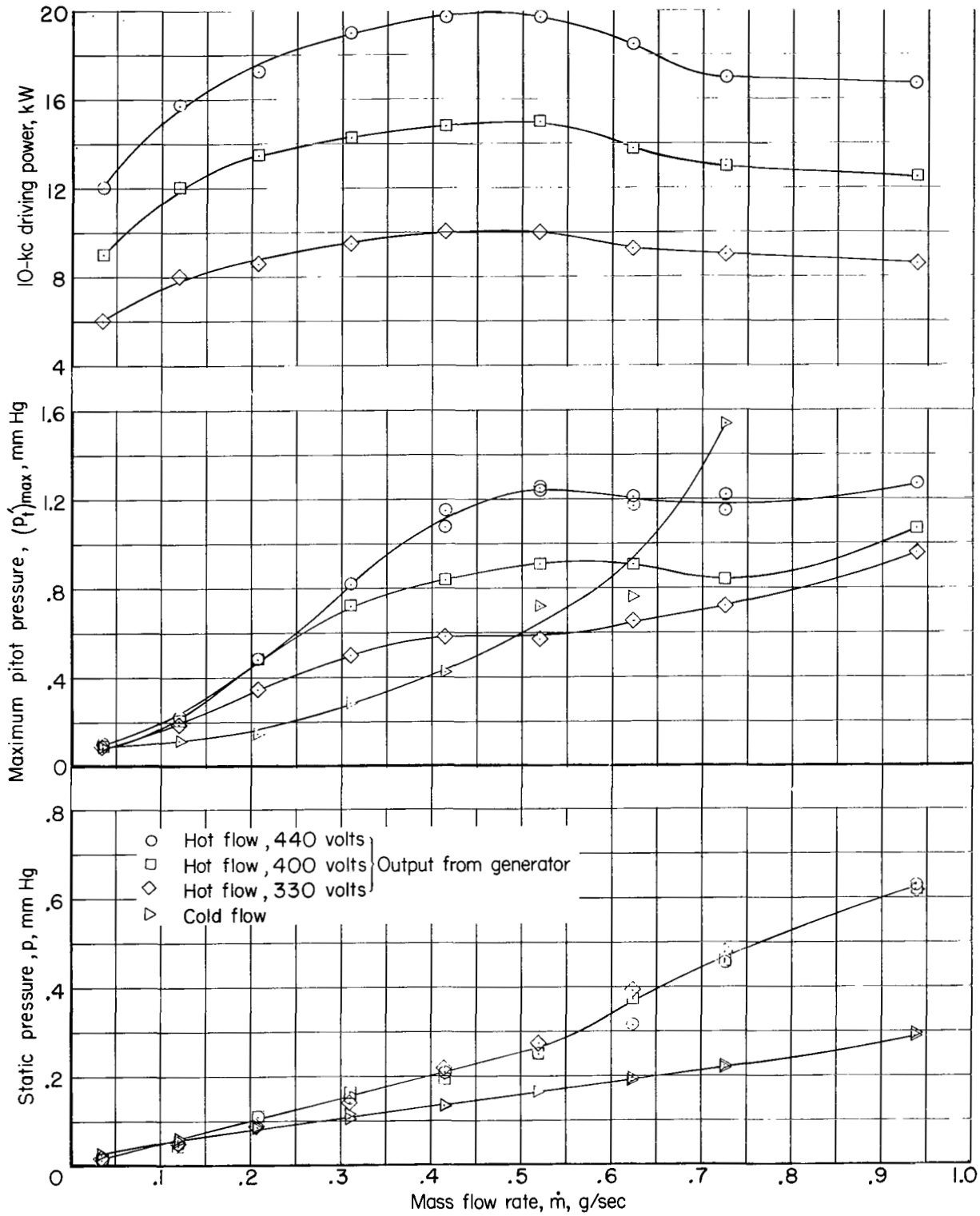

Figure 5. - Variation of 10-kc driving power, maximum pitot pressure, and static wall pressure with mass flow rate in the 15-cm-diameter plasma accelerator.

resulted in an increase in power output of approximately 100 percent. It is apparent that the power drawn varies approximately as the square of the applied voltage. At a constant voltage setting, the maximum power occurred at a mass flow rate of approximately 0.45 g/sec and the power decreased as the mass flow rate and the pressure were reduced. This reduction in power is consistent with the result reported in reference 16 in an induced discharge. The power drawn depends on such factors as the intensity of the discharge, the pressure, and the speed of the plasma.

The static pressure measured at the wall of the 15-cm accelerator is also shown in figure 5. When the accelerator was energized, the static pressure increased, except for mass flow rates below 0.12 g/sec. The increase in static pressure is due to an increase in gas temperature. From a mass flow rate of 0.55 g/sec and a static pressure of approximately 0.30 mm Hg, the rise in static pressure increased appreciably with an increase in mass flow rate. This abrupt rise occurs at the approximate pressure that the hot flow is changing from the slip-flow region to continuum flow. At the higher mass flow rates and higher pressures, the mean free path decreased and the collision frequency between the charged particles and the neutral gas increased with the result that the charged particles lose their directed motion and assume a random motion more rapidly than at low pressure, which causes an increase in the gas heating rate.

Increasing the 10-kc voltage from 330 volts to 440 volts had a relatively small effect on the static pressure at a given mass flow rate (fig. 5). However, the increase in voltage caused an appreciable increase in the maximum pitot pressure, from about 130 percent to approximately 250 percent of the cold-flow value at a mass flow rate of 0.425 g/sec as the power varied from 10 to 20 kW. The largest increase in the maximum pitot pressures at each voltage level was 0.22 mm Hg at 330 volts, 0.44 mm Hg at 400 volts, and 0.68 mm Hg at 440 volts as the 10-kc power was increased from 9.5 kW to 14.5 kW to 19.8 kW, respectively. It appears that the largest increase in the maximum pitot pressures at each voltage level is approximately proportional to the increase in power.

With an increase in voltage, the ratio of pitot pressure to static pressure also increased, as shown in figure 6; this indicates an increase in Mach number and velocity with increasing voltage. The increase in Mach number would normally occur in continuum flow with a decrease in the static pressure and static temperature. However, adding heat energy to a supersonic flow downstream from the throat tends to increase the static temperature and the static pressure and to decrease the Mach number. Since, at a given mass flow rate, the static pressure remained approximately constant and the Mach number increased, it is evident that the major part of the additional power - that is, the increase in power resulting from raising the supply voltage from 330 volts to 440 volts - contributed to the directed motion rather than to the thermal motion.

At each voltage level there is a mass-flow range for the 15-cm accelerator within which the hot-flow pressure ratio is greater than the cold-flow value. With an increase in voltage this mass-flow range extended to higher mass flow rates. In general, it appears that with a power supply having a higher voltage and power capability, the region of acceleration could be extended to higher pressures.

The pressure ratio (fig. 6) increased at the two high voltages (400 and 440 volts) when the mass flow rate of the accelerator was decreased below 0.12 g/sec; this increase indicated an increase in Mach number. The indicated increase in pressure ratio is partly due to viscous effects on the pitot-pressure tube at low Reynolds number. However, viscous effects account at most for an increase in pressure ratio of about 25 percent, according to references 14 and 15. Therefore, this increase in pressure ratio demonstrates that a larger percentage of the power in the discharge is going into directed motion, rather than thermal motion, at mass flow rates below 0.12 g/sec. At the higher mass flow rates where the pressure ratio for the hot flow is less than that for the cold flow, the opposite effect occurs - that is, a higher percentage of the power in the discharge goes into thermal motion rather than into directed motion with a resultant reduction in Mach number and an increase in static temperature.

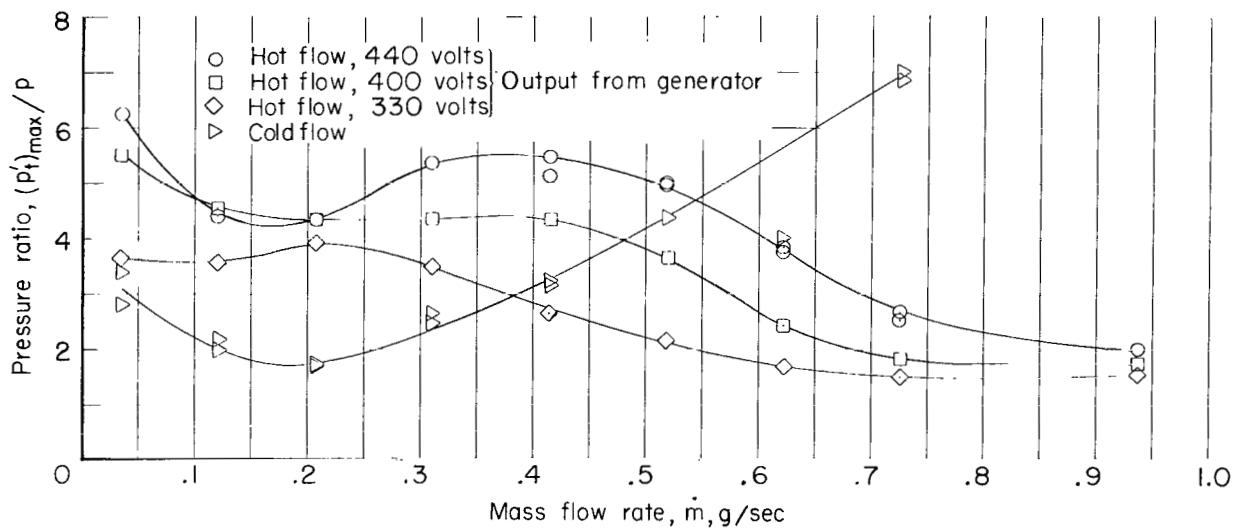

Figure 6.- Variation of the ratio of maximum pitot pressure to static pressure with mass flow rate in the 15-cm-diameter plasma accelerator.

Velocity Measurements

The charged-particle velocities, obtained with a pair of photomultipliers placed along the direction of the stream in the 15-cm accelerator, exhibited good repeatability at the mass flow rates between 0.2 g/sec to 0.72 g/sec (fig. 7). At mass flow rates less than 0.2 g/sec, the charged-particle velocities did not exhibit good repeatability and from the appearance of the photomultiplier records the accelerator was beginning to operate erratically.

The charged-particle velocities increased from 4,000 m/sec to 20,000 m/sec as the mass flow rate was reduced from 0.725 g/sec to 0.035 g/sec. The increase in velocity as the mass flow rate is reduced (fig. 7) is directly related to the increase in mean free path with decreasing mass flow rate (fig. 8). The gas flow is in the transition region from slip flow to free-molecule flow at the lower mass flow rates, and the collision frequency between the charged particles and the neutral gas has decreased. Hence, the charged particles retain a high percentage of their directed motion and attain high velocities.

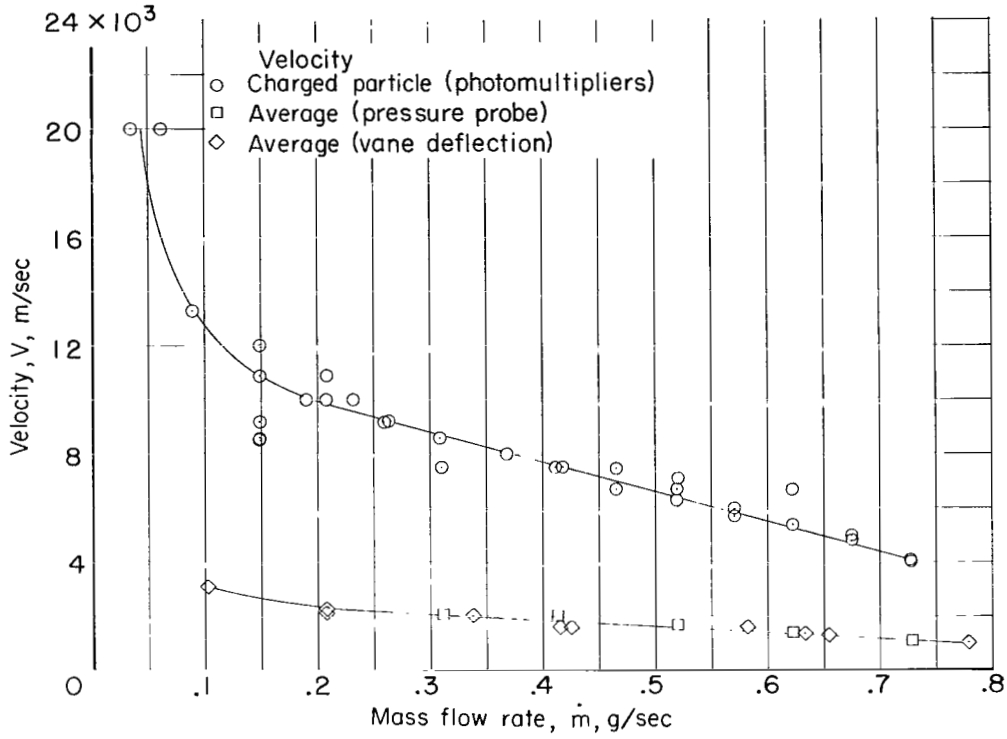

Figure 7. - Variation of velocity with mass flow rate in the 15-cm-diameter plasma accelerator. Output from generator, 440 volts; p_t = 5 to 40 mm Hg; p = 0.016 to 0.470 mm Hg; A^* = 0.57 cm^2.

The average velocities of the neutral gas and the charged particles, shown in figure 7, were obtained from the pitot-pressure profiles and the vane deflections. For a constant driving voltage, the average velocities were about 25 percent of the charged-particle velocities in the 15-cm accelerator and remained approximately constant over the mass-flow range studied. However, the 10-kc power input, shown in figure 5, decreased at low mass flow rates and pressures. If the power level attained at mass flow rates of about 0.45 g/sec could be maintained at low mass flow rates, the percentage of ionization would have to increase and the average velocities would then approach the charged-particle velocities. In order to realize this condition, a power supply having a greater voltage capability would be required. The limitations of the 10-kc-motor generator are discussed in reference 3.

The 15-cm accelerator was operating somewhat erratically at mass flow rates below 0.20 g/sec, possibly as a result of the loss of ionization by diffusion to the walls at low pressures. In order to reduce the ionization losses to the walls as well as the frictional losses and to increase the induced voltage, the 10-cm accelerators were constructed with a shorter duct between the nozzle throat and the vacuum chamber, as shown in figure 2.

The 10-cm accelerators operated at mass flow rates below those of the 15-cm accelerator, and the velocity measurements exhibited better repeatability

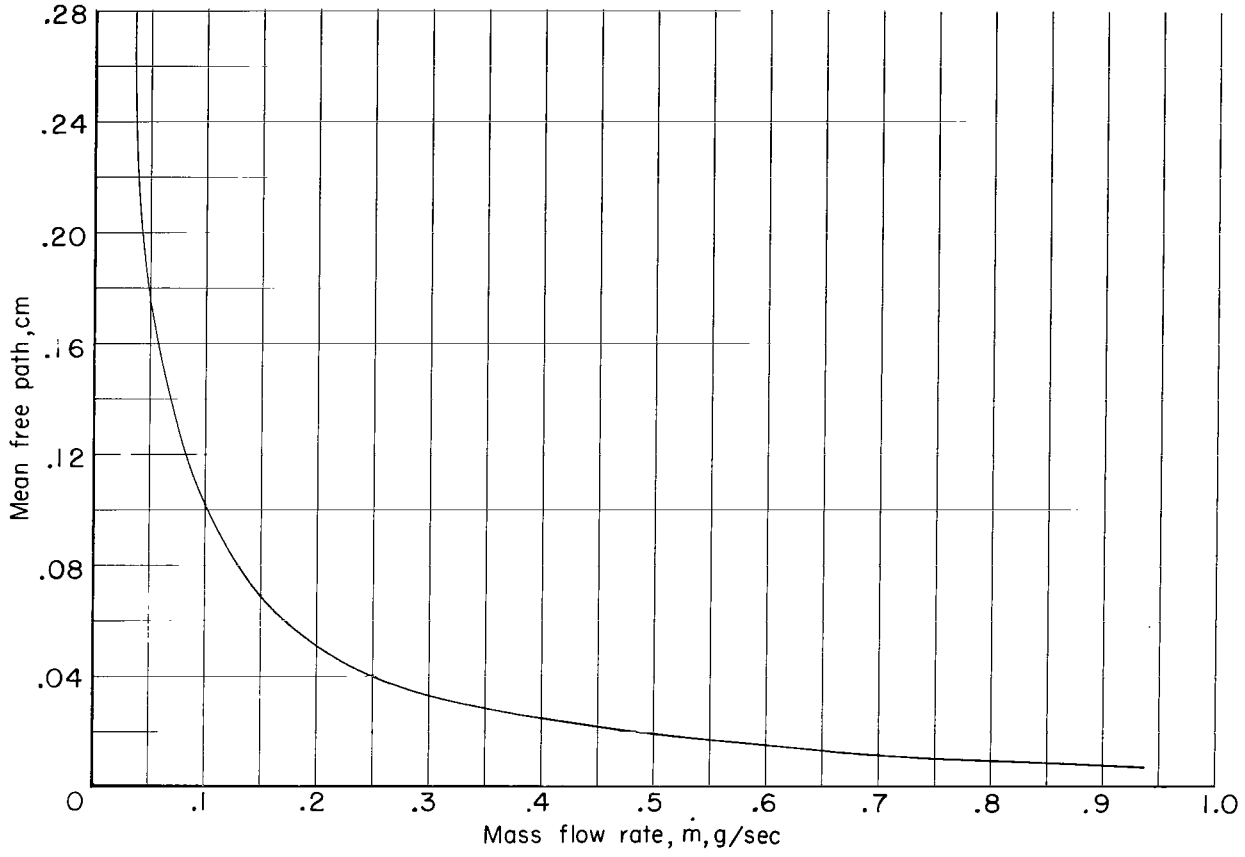

Figure 8. - Variation of the mean free path of the neutral particles with mass flow rate in the 15-cm-diameter plasma accelerator with 440-volt output from generator.

at the low mass flow rates. (See figs. 7 and 9.) A typical photomultiplier record is shown in figure 10(a) for the 10-cm accelerators. At mass flow rates less than 0.007 g/sec, the 10-cm accelerators operated erratically as shown by the photomultiplier record in figure 10(b). This erratic operation is similar to that of the 15-cm accelerator at low mass flow rates and is apparently due to the failure of the plasma to conduct uniformly on every cycle at low pressures. If the mass flow rate is reduced further, the accelerator begins to turn on and off very rapidly in a fraction of a millisecond until it stops operating when the voltage available cannot sustain the discharge at the low pressure.

At mass flow rates above approximately 0.05 g/sec, the photomultiplier records indicate a fluctuation in the flow, as shown in figure 10(c). The fluctuation in the flow was verified by high-speed motion pictures at 7,500 frames per second which indicated that the discharge was fluctuating circumferentially and may be similar to the phenomena that occurred in reference 2 in a pulse-type accelerator. When the accelerator was operating in this fluctuating condition, the results were ambiguous and no charged-particle-velocity measurements were obtained.

Figure 9 shows that the charged-particle velocities in the 10-cm accelerators exhibited the same characteristic discussed for the charged-particle velocities in the 15-cm accelerator - namely, the velocity increased as the mass flow rate was reduced. However, higher velocities were generally obtained in the 10-cm accelerators. The charged-particle velocity increases approximately as the fourth root of the generator power output (figs. 9(b) and 9(c)); this is consistent with the theory of reference 17. The highest velocities were obtained in the 10-cm accelerator with the smallest throat area and the largest pressure ratio (fig. 9(a)). The maximum charged-particle velocity was 40,000 m/sec at a mass flow rate of approximately 0.01 g/sec.

Thrust

The momentum thrust and the total thrust in the 15-cm accelerator are shown in figures 11(a) and 11(b), respectively. For comparison, the ideal thrust F_i that would be obtained if the entire flow were moving at the charged-particle velocity was calculated and is also shown in figure 11. In general, the momentum thrust (fig. 11(a)) increased with increasing mass flow rate until it reached a maximum at about 0.60 g/sec and then it began to decrease.

The general effect of adding the pressure thrust to the momentum thrust (fig. 11(b)) was small at low mass flow rates but increased appreciably at high mass flow rates because of the increase in pressure. The pressure increase caused the hot-flow total thrust to continue to increase with increasing mass flow rate to a value of about 14×10^4 dynes at the highest mass flow rate of 0.78 g/sec. The highest ideal thrust F_i occurred at a mass flow rate of 0.60 g/sec and was about 39×10^4 dynes, whereas the actual thrust from the pressure and vane measurements was about 14×10^4 dynes or 36 percent of the highest value of F_i. Pressure and vane measurements were not obtained at mass flow rates below 0.10 g/sec, where the charged-particle velocity was about 20,000 m/sec. If a linear variation of thrust with mass flow rate is assumed in figure 11(b), the total thrust would be approximately 2×10^4 dynes at a mass flow rate of 0.05 g/sec.

The variation of the ideal thrust F_i with mass flow rate in the 10-cm accelerator is shown in figure 12. The momentum thrust is not shown separately since the data for the 10-cm accelerators were obtained at low pressures and the pressure thrust was small. In general, the ideal thrust F_i increased with increasing mass flow rate, corresponding to the variation in thrust with mass flow rate in the 15-cm accelerator at low mass flow rates (fig. 11). The thrust F_i was highest in the 10-cm accelerator with the smallest throat area (fig. 12(a)) and varied from 2.5×10^4 dynes to 8.7×10^4 dynes as the mass flow rate varied from 0.007 g/sec to about 0.058 g/sec. At the maximum charged-particle velocity of 40,000 m/sec in the 10-cm accelerator, the thrust F_i shown in figure 12(a) at a mass flow rate of 0.007 g/sec is approximately 2.5×10^4 dynes. No pressure or vane measurements were obtained in the 10-cm accelerator and, therefore, the actual thrust is not known. If the thrust is assumed to be approximately 30 percent of F_i as for the 15-cm accelerator at the low mass flow rates, the actual thrust would be approximately 7×10^3 dynes at a mass flow rate of 0.007 g/sec.

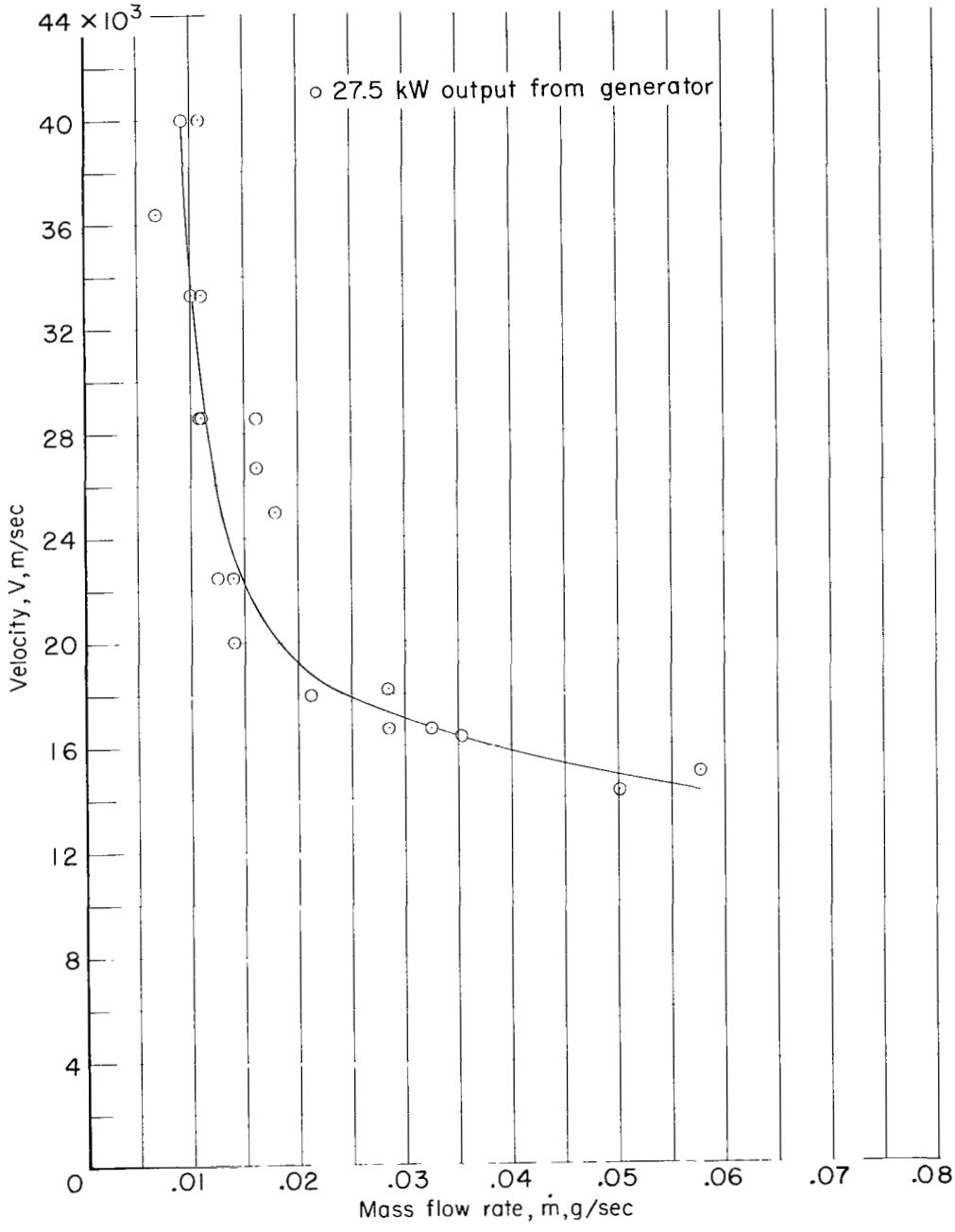

(a) $A^* = 0.31\ cm^2$; $p_t = 1.52$ to 11.7 mm Hg; $p \approx 0.003$ to 0.028 mm Hg.

Figure 9. - Variation of charged-particle velocity with mass flow rate in the 10-cm-diameter plasma accelerators.

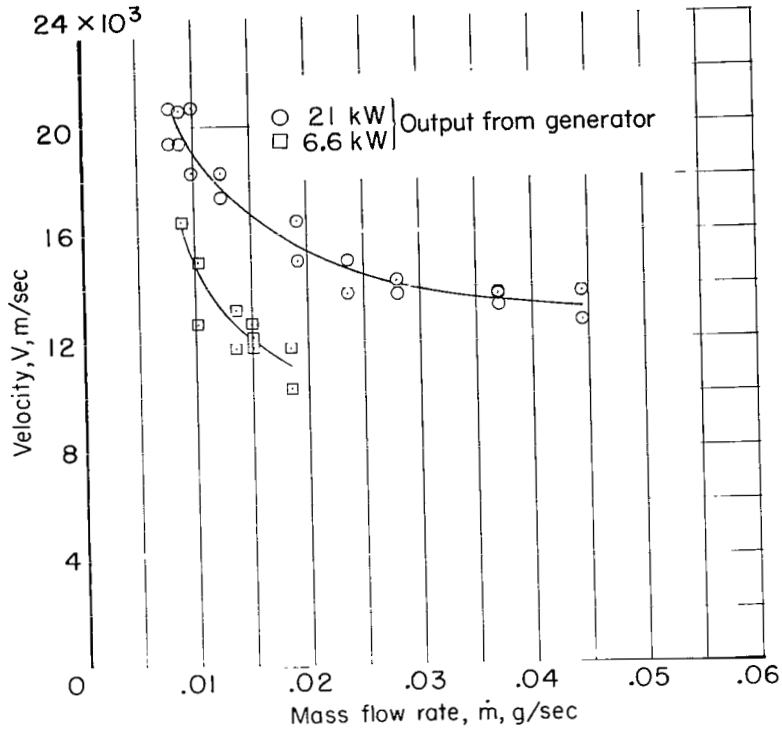

(b) A^* = 0.51 cm^2; p_t = 1.25 to 5.0 mm Hg; $p \approx$ 0.005 to 0.024 mm Hg.

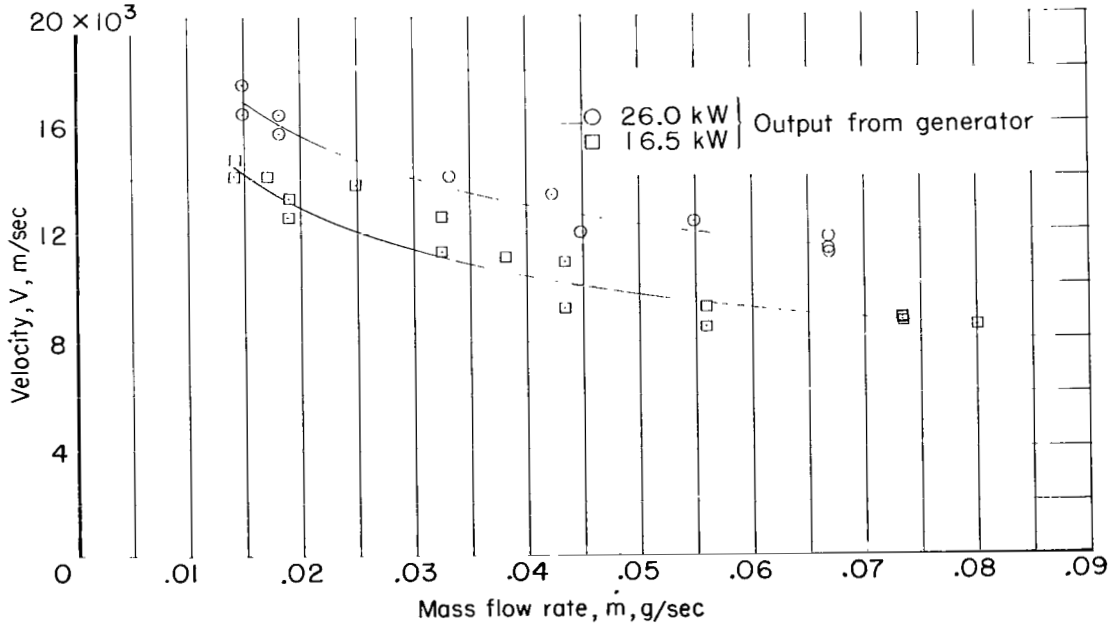

(c) A^* = 4.25 cm^2; p_t = 0.175 to 1.20 mm Hg; $p \approx$ 0.010 to 0.060 mm Hg.

Figure 9. - Concluded.

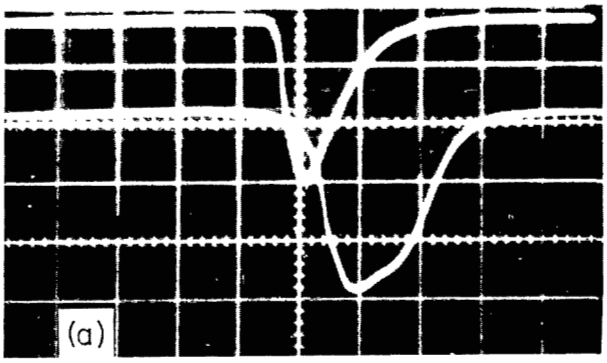

(a) $\dot{m}$ = 0.0098 g/sec; p_t = 1.78 mm Hg; p = 0.010 mm Hg; A^* = 0.51 cm^2; oscilloscope sweep, 5 μsec/cm.

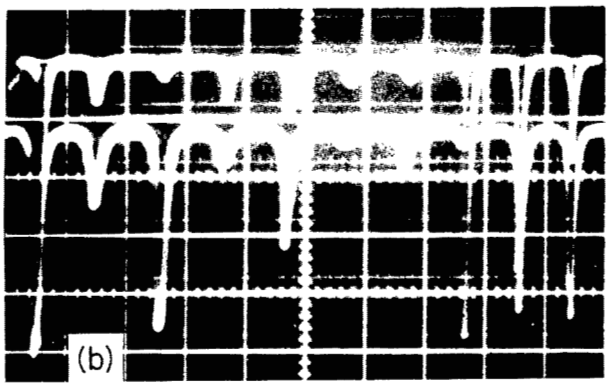

(b) $\dot{m}$ = 0.0051 g/sec; p_t = 1.03 mm Hg; p = 0.003 mm Hg; A^* = 0.31 cm^2; oscilloscope sweep, 50 μsec/cm.

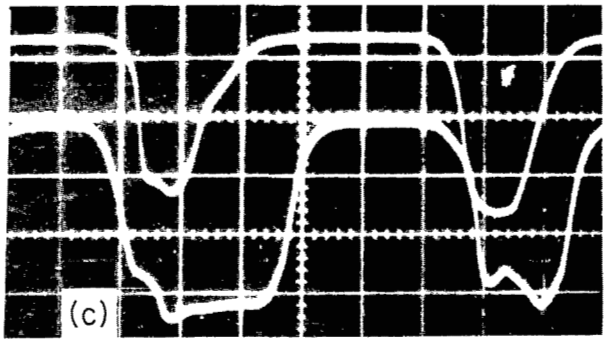

(c) $\dot{m}$ = 0.110 g/sec; p_t = 9.50 mm Hg; p = 0.046 mm Hg; A^* = 0.51 cm^2; oscilloscope sweep, 10 μsec/cm.

Figure 10. - Typical oscilloscope traces obtained from 10-cm-diameter plasma accelerators with two photomultipliers placed longitudinally along the direction of flow. Photomultiplier spacing, 8.25 cm; power output from generator, 26 kW.

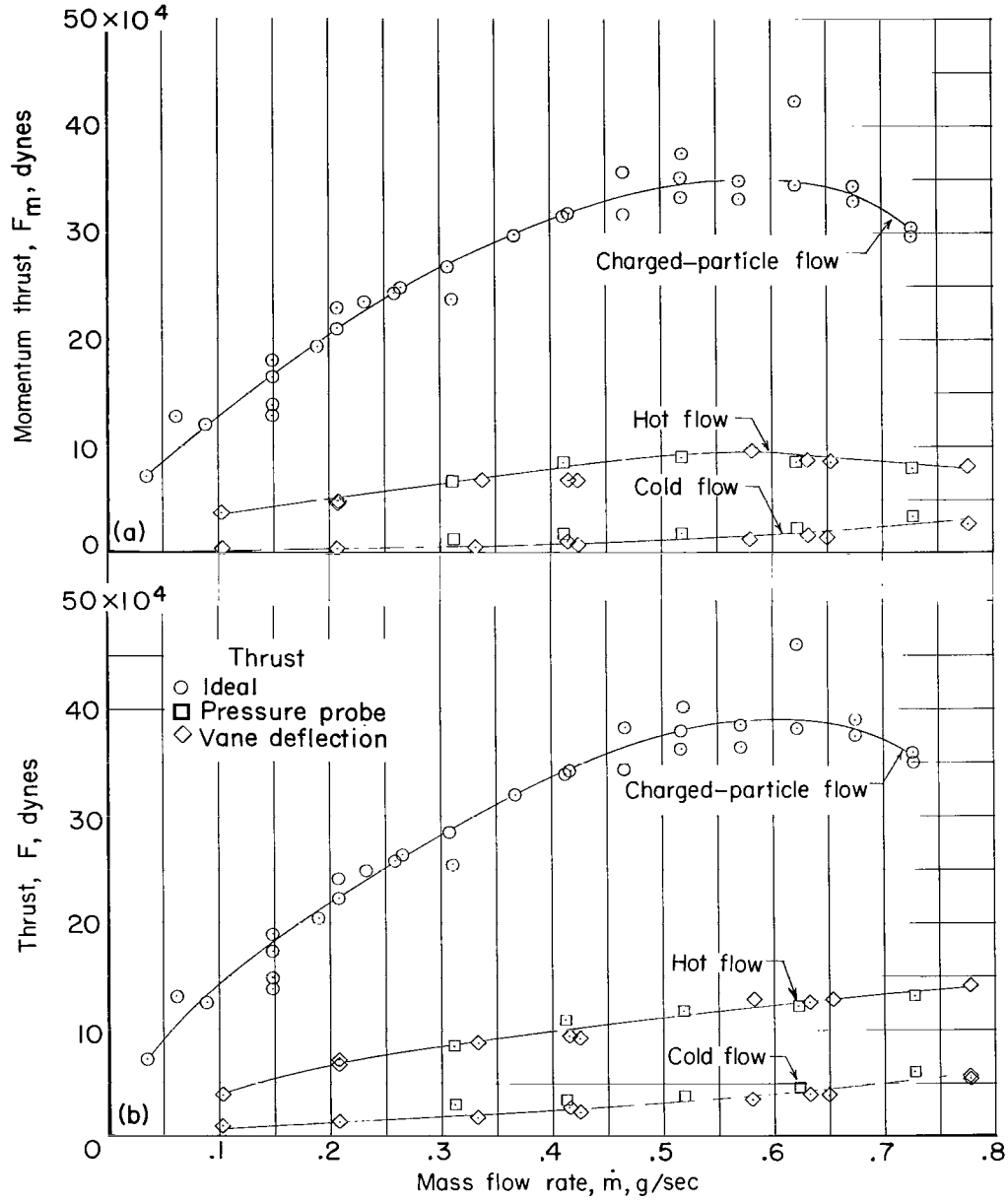

(a) Momentum thrust.

(b) Total thrust.

Figure 11. - Variation of thrust with mass flow rate in the 15-cm-diameter plasma accelerator with 440-volt output from generator.

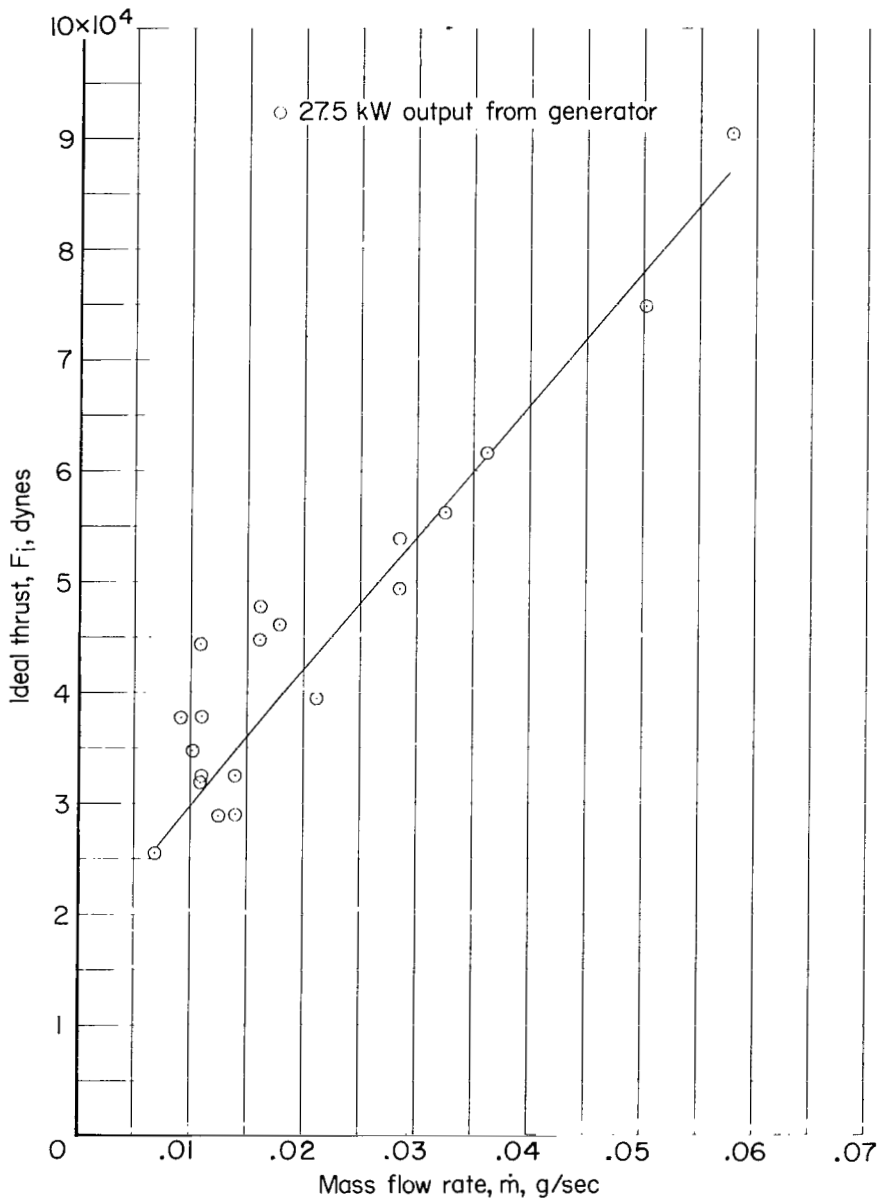

(a) $A^* = 0.31\ cm^2$.

Figure 12. - Variation of the ideal thrust with mass flow rate in the 10-cm-diameter plasma accelerators.

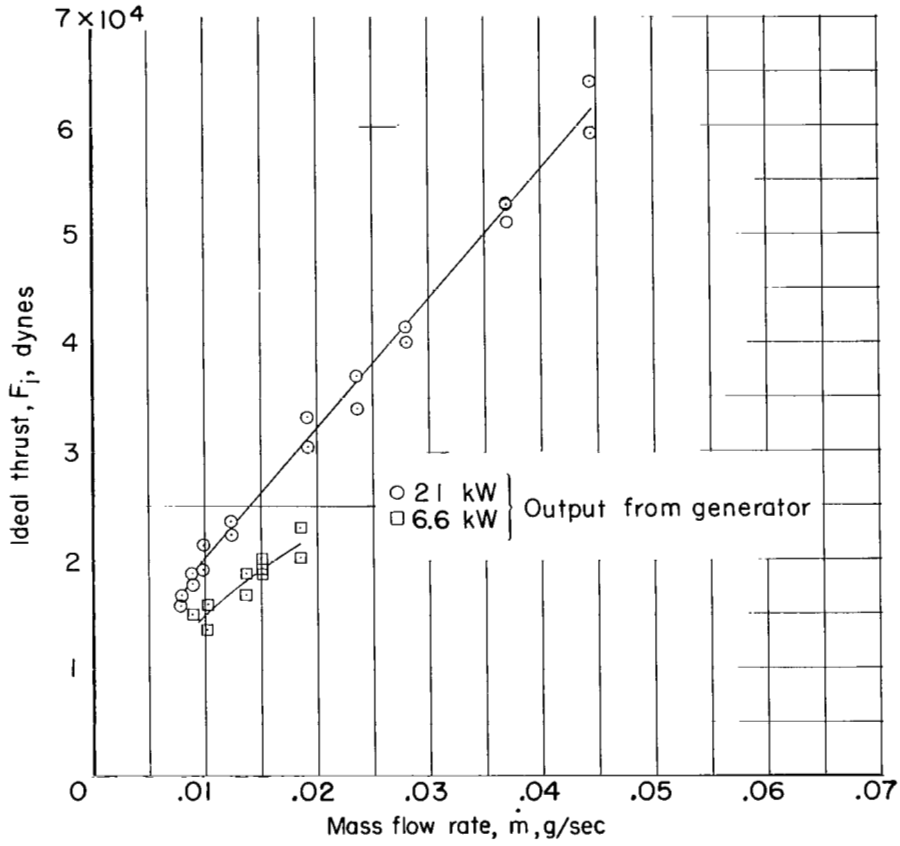

(b) $A^* = 0.51\ cm^2$.

Figure 12. - Continued.

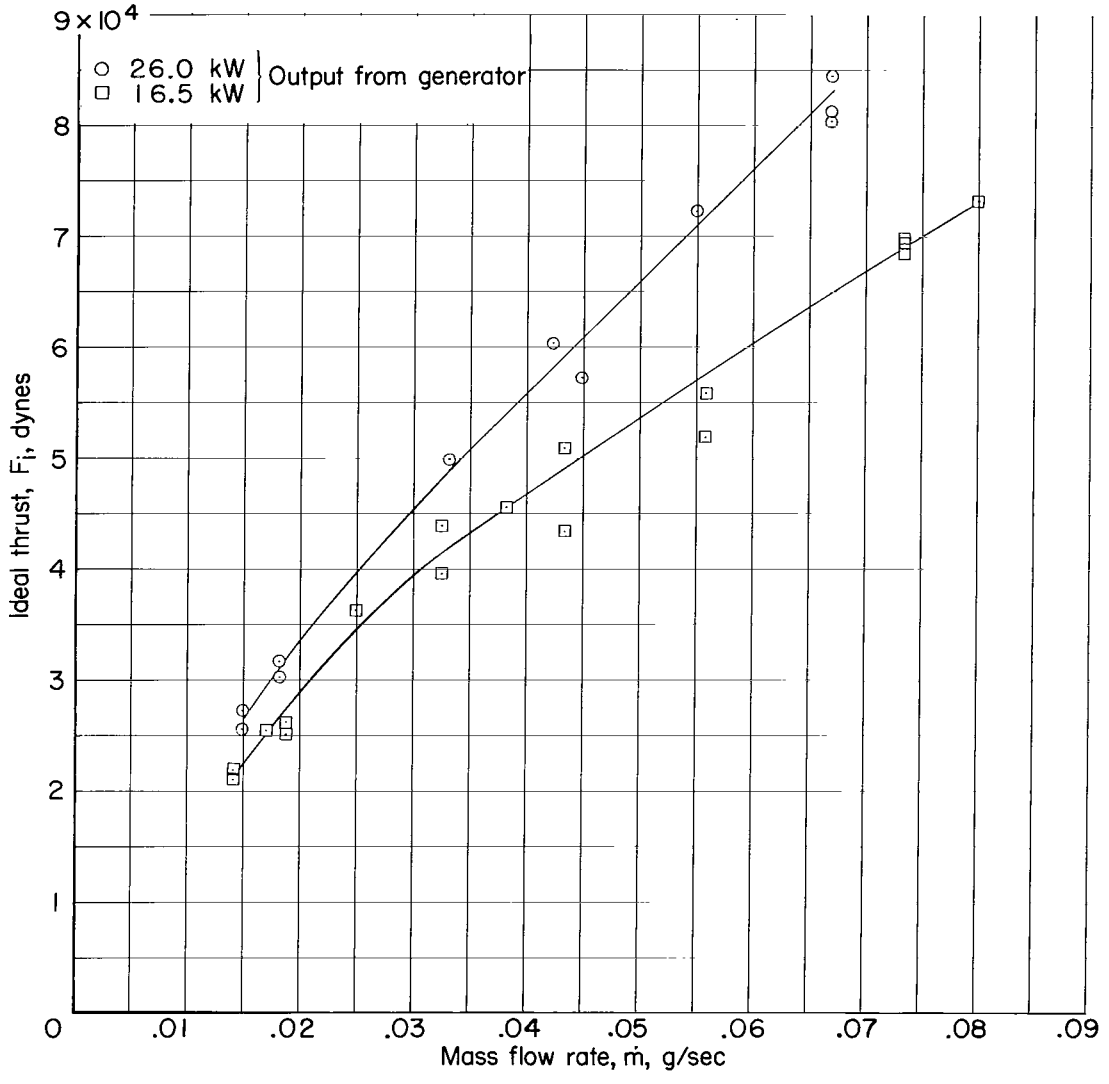

(c) $A^* = 4.25\ cm^2$.

Figure 12. - Concluded.

CONCLUDING REMARKS

From an experimental investigation of continuous-flow induction plasma accelerators using a 10-kc driving coil on supersonic nozzles, the following remarks are indicated:

At low mass flow rates, the pitot pressure increased over the cold-flow value when the accelerator was turned on. The maximum increase obtained was 250 percent. At high mass flow rates and pressures, the heating of the supersonic flow was sufficient to lower the Mach number. Pressure-probe measurements indicated that the entire flow, including the boundary layer and separated-flow region, was accelerated.

Direct velocity measurements with photoelectric detectors indicated that the charged-particle velocities increased as the mass flow rate was reduced and as the power was increased. For a constant driving voltage, the average velocity was about 25 percent of the charged-particle velocity in the 15-cm-diameter accelerator and remained virtually constant over the mass-flow range studied. The maximum charged-particle velocity was 20,000 m/sec in the 15-cm-diameter accelerator and 40,000 m/sec in the 10-cm-diameter accelerator.

Values of average velocity and thrust obtained from vane measurements compared well with those obtained from pressure measurements. The maximum actual thrust obtained was 14×10^4 dynes.

At mass flow rates below 0.007 g/sec the accelerator operation became erratic, apparently a failure of the plasma to conduct uniformly on every cycle at low pressures. In the 10-cm-diameter accelerators, at mass flow rates above 0.05 g/sec there was evidence of a circumferential fluctuation in the flow.

The trend of the data indicates that, with a power supply having a higher voltage and power capability, higher velocities and thrusts could be produced and that the region of acceleration could be extended to higher pressures.

Langley Research Center,
National Aeronautics and Space Administration,
Langley Station, Hampton, Va., September 18, 1964.

REFERENCES

1. Ziemer, Richard W.: Electromagnetic Shock Tubes. Dynamics of Conducting Gases, Ali Bulent Cambel and John B. Fenn, eds., Northwestern Univ. Press, c.1960, pp. 139-149.

2. Hart, Philip J.: Plasma Acceleration With Coaxial Electrodes. Phys. Fluids, vol. 5, no. 1, Jan. 1962, pp. 38-47.

3. Barger, R. L.; Brooks, J. D.; and Beasley, W. D.: The Design and Operation of a Continuous-Flow Electrodeless Plasma Accelerator. NASA TN D-1004, 1962.

4. Jones, Robert E.; and Palmer, Raymond W.: Traveling Wave Plasma Engine Program at NASA Lewis Research Center. Third Symp. Eng. Aspects of Magnetohydrodynamics, Univ. of Rochester, Mar. 28-30, 1962.

5. Fonda-Bonardi, G.: The Use of an Electrodeless Plasma Accelerator as a Hypersonic Wind Tunnel. Advances in Hypervelocity Techniques, Arthur M. Krill, ed., Plenum Press, 1962, pp. 129-144.

6. Barger, R. L.; Brooks, J. D.; and Beasley, W. D.: An Experimental Study of Continuous Plasma Flows Driven by a Confined Arc in a Transverse Magnetic Field. NASA TN D-716, 1961.

7. Carter, Arlen F.; Wood, George P.; Sabol, Alexander P.; and Weinstein, Richard H.: Experiments in Steady-State High-Density Plasma Acceleration. Engineering Aspects of Magnetohydrodynamics, Clifford Mannal and Norman W. Mather, eds., Columbia Univ. Press, 1962, pp. 45-55.

8. Enkenhus, K. R.: The Design, Instrumentation and Operation of the UTIA Low Density Wind Tunnel. Rept. No. 44 (AFOSR-TN-58-22, AD 148 061), Inst. Aerophys., Univ. of Toronto, June 1957.

9. Beasley, W. D.; Brooks, J. D.; and Barger, R. L.: Direct Velocity Measurements in Low-Density Plasma Flows. NASA TN D-1783, 1963.

10. Guthrie, A.; and Wakerling, R. K.: Vacuum Equipment and Techniques. McGraw-Hill Book Co., Inc., 1949, pp. 5 and 249.

11. Rodriguez, Charles J.: An Experimental Investigation of the Effect of High-Pressure Tailpipe Length on the Performance of Solid-Propellant Motors for Rocket-Powered Aircraft. NACA RM L52E12a, 1952.

12. McBee, Warren D.: A Study of the Influence of a Strong Transverse Magnetic Field on an Unconfined Glow Discharge in Air at About 1 mm Pressure. Ph. D. Dissertation, Univ. of Michigan, 1951.

13. Page, Leigh; and Adams, Norman Ilsley, Jr.: Principles of Electricity. Third ed., D. Van Nostrand Co., Inc., c.1958, pp. 329-330.

14. Enkenhus, K. R.: Pressure Probes at Very Low Density. Rept. No. 43 (AFOSR-TN-57-237, AD 126 534), Inst. Aerophys., Univ. of Toronto, Jan. 1957.

15. Bailey, A. B.; and Boylan, D. E.: Some Experiments on Impact-Pressure Probes in a Low-Density, Hypervelocity Flow. AEDC-TN-61-161 (Contract No. AF 40(600)-800 S/A 24(61-73), Arnold Eng. Develop. Center, Dec. 1961.

16. Cabannes, François: Étude dé la décharge électrique par induction dans les gaz rares. Ann. Phys. (Paris), ser. 12, vol. 10, Nov.-Dec. 1955, pp. 1026-1078.

17. Matthews, Clarence W.: A Theoretical Study of the Motion of an Idealized Plasma Ring Under the Influence of Various Coaxial Magnetic Fields. NASA TR R-121, 1961.

"The aeronautical and space activities of the United States shall be conducted so as to contribute . . . to the expansion of human knowledge of phenomena in the atmosphere and space. The Administration shall provide for the widest practicable and appropriate dissemination of information concerning its activities and the results thereof."

—NATIONAL AERONAUTICS AND SPACE ACT OF 1958

NASA SCIENTIFIC AND TECHNICAL PUBLICATIONS

TECHNICAL REPORTS: Scientific and technical information considered important, complete, and a lasting contribution to existing knowledge.

TECHNICAL NOTES: Information less broad in scope but nevertheless of importance as a contribution to existing knowledge.

TECHNICAL MEMORANDUMS: Information receiving limited distribution because of preliminary data, security classification, or other reasons.

CONTRACTOR REPORTS: Technical information generated in connection with a NASA contract or grant and released under NASA auspices.

TECHNICAL TRANSLATIONS: Information published in a foreign language considered to merit NASA distribution in English.

TECHNICAL REPRINTS: Information derived from NASA activities and initially published in the form of journal articles.

SPECIAL PUBLICATIONS: Information derived from or of value to NASA activities but not necessarily reporting the results of individual NASA-programmed scientific efforts. Publications include conference proceedings, monographs, data compilations, handbooks, sourcebooks, and special bibliographies.

Details on the availability of these publications may be obtained from:

SCIENTIFIC AND TECHNICAL INFORMATION DIVISION

NATIONAL AERONAUTICS AND SPACE ADMINISTRATION

Washington, D.C. 20546